Piezo-Phototronic Effect-Induced Dual-Mode Light and Ultrasound Emissions from ZnS:Mn/PMN–PT Thin-Film Structures

*Yang Zhang, Guanyin Gao, Helen L.W. Chan, Jiyan Dai, Yu Wang, and Jianhua Hao**

The phenomenon of electroluminescence (EL) has attracted an ever-increasing demand for applications throughout the illumination and display industries.[1–5] In EL devices, light generation in light-emitting diodes (LEDs) is mostly investigated for flat-panel display and light sources due to their high brightness, long lives, and low power consumption.[6–9] It is well-known that the LED is essentially a p–n junction diode typically made from a semiconductor. The light emission is generated by the direct injection and subsequent recombination of electron–hole pairs in the forward-biased p–n junction.[10] The phenomenon of light emission from electron–hole pair recombination as a result of minority carrier injection is regarded as injection EL. It is somewhat surprising that very limited work on exploiting EL devices beyond the p–n junction structure has been reported in recent decades. In order to search for more EL device types, an important question in this area – both scientifically and technologically – is how to tailor the material properties and therefore construct a new device structure. Particularly, it would be very attractive if the light source could generate an additional signal, offering a novel multi-modal functional source.

An emerging field – so-called piezo-phototronics – recently proposed by Wang is of particular interest.[11] Piezo-phototronics derive from the term "piezotronics", which means utilizing strain-induced piezoelectric potential to tune and gate the charge transport behavior for fabricating new functional devices.[12,13] Furthermore, the piezoelectric potential utilized in optoelectronic devices results in piezo-phototronics. The functionalities of piezotronic and piezo-photronic devices – ranging from nanogenerators[14–16] and field-effect transistors[17,18] to photosensors[19] and piezoelectric diodes[20,21] – are ultimately based on the intricate coupling of piezoelectric, semiconducting, and photonic characteristics. Previous works on piezo-phototronics are limited to one-dimensional (1D) nanostructure. Hence, it is much needed to know whether this new concept is applicable to other device configurations. Here, we report the fabrication and characteristics of strain-induced piezoelectric potential stimulated luminescence from ZnS:Mn film grown on piezoelectric $Pb(Mg_{1/3}Nb_{2/3})O_3$–$x$$PbTiO_3$ (PMN–PT) substrate. Compared with 1D nanostructures, the utilization of a thin-film structure would be beneficial in terms of increasing device reproducibility and reducing the fabrication cost, because of the mature thin-film fabrication technologies available. Additionally, a thin-film structure facilitates the integration and patterning of devices. More importantly, the simultaneous generation of light and ultrasound waves using a single system is demonstrated for the first time in this work. We can tune the luminescence and ultrasound signal of the ZnS:Mn films via a converse piezoelectric effect in PMN–PT upon the application of either an ac or a dc electric-field. Such a multifunctional source may find applications in a variety of systems. For instance, a variety of techniques such as high-frequency ultrasound imaging and fluorescence spectroscopy have been widely used for medical diagnosis. However, each of these techniques has intrinsic advantages and deficiencies. There is a trend to develop a combined approach capable of evaluating structural characteristics as well as biochemical properties, which may provide higher predictive and complementary information compared to a single approach, either by optical or ultrasound methods.[22] Therefore, the integration of novel dual-modal source combining light-emission and ultrasound generation on a single wafer here with detecting system will be very helpful in developing a hybrid system for tissue diagnosis.

The basic strategy for the fabrication of an integrated source combining luminescent and ultrasonic characteristics is shown in **Figure 1**. ZnS:Mn selected here is a commonly used phosphor layer in alternating current thin-film electroluminescent (ACTFEL) devices.[23,24] The wurtzite-type Mn^{2+} doped ZnS can also possess a non-central symmetric structure and inherently exhibit piezoelectric characteristics. The piezoelectric potential has been proven to be capable of modifying the band structure significantly in the presence of strain.[11–21] Analogously, a piezoelectric potential can be induced by the strain from a PMN–PT substrate, as shown in Figure 1, which is regarded as the fuse to trigger the luminescent center Mn^{2+}. A commercial ferroelectric (001)-oriented PMN–PT single-crystal (Hefei Kejing Material Technology Co., Ltd.) was chosen as substrate due to its outstanding ferroelectric polarization and converse piezoelectric effects.[25] PMN–PT single crystals have been extensively used to the strain-related characteristics of various samples.[26,27] PMN–PT single-crystals feature large piezoelectric coefficients and extraordinary high electromechanical coupling factors, these merits translate into high performance of ultrasound transducers fabricated with PMN–PT single crystals.[28]

The ZnS:Mn thin film was grown on PMN–PT by pulsed laser deposition. The x-ray diffraction (XRD) pattern of the ZnS:Mn

Y. Zhang, Dr. G. Y. Gao, Prof. H. L.W. Chan, Dr. J. Y. Dai, Dr. Y. Wang, Dr. J. H. Hao
Department of Applied Physics and Materials Research Center
The Hong Kong Polytechnic University
Hung Hom, Kowloon, Hong Kong, P. R. China
E-mail: apjhhao@polyu.edu.hk

DOI: 10.1002/adma.201104584

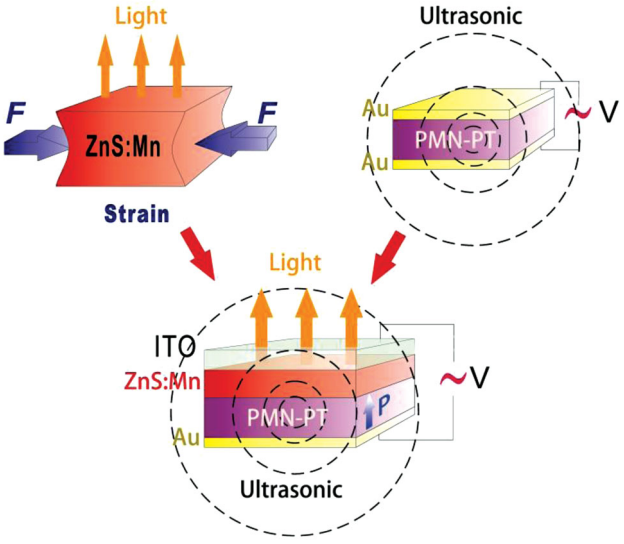

Figure 1. The setup used for measuring the luminescent and ultrasonic characteristics of ZnS:Mn film grown on PMN–PT substrate under an ac electric- field.

film on PMN–PT substrate is shown in **Figure 2**a. Only (00*l*) diffraction peaks were observed in a wide-angle range from 20° to 70°, indicating the film to have a good *c*-axis preferred orientation. The lattice constant *c* is measured to be 6.492 Å, which is larger than that in bulk ZnS, *c* = 6.257 Å, JCPDS#36-1450 (Joint Committee on Powder Diffraction Standards). The lattice expansion in the film may result from the existence of sulfur vacancies in the samples. To further investigate the microstructure of the ZnS:Mn films on PMN–PT (001), cross-sectional transmission electron microscopy (TEM) studies have been carried out on the interface of the sample. Figure 2b is a low-magnification, brightfield TEM image of the sample. A transparent electrode of indium tin oxide (ITO) was deposited on top, and light emission can pass through the ITO layer. The thicknesses of ITO electrode and ZnS:Mn film are about 300 and 600 nm, respectively. The ZnS:Mn film has a smooth surface, uniform thickness, and clearly defined interface with the (001) PMN–PT substrate. The crystallographically textured film is in the form of columnar crystallites, with their long axes perpendicular to the substrate. Figure 2c shows a high-resolution TEM image for the ZnS:Mn/PMN–PT interface of the sample. It is clearly seen that there are some dislocations formed at the interface, and a nanograin of ZnS:Mn formed in the film, confirming the textured crystallization of the film on (001) PMN–PT substrate.

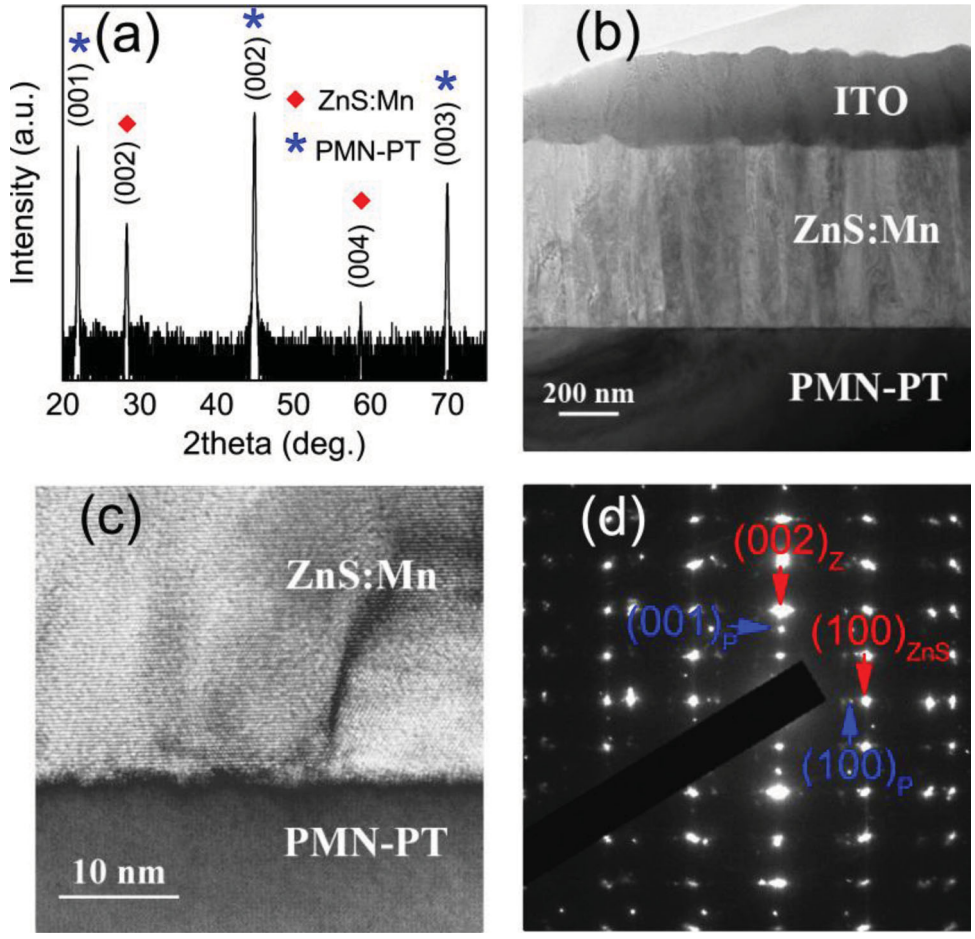

Figure 2. Structural characterization of the ZnS:Mn film grown on (001)-oriented PMN–PT single-crystal substrate. a) X-ray diffraction θ–2θ scans. b) Low magnitude brightfield image. c) High-resolution TEM image for the interface structures. d) SAED pattern.

A selected area electron diffraction (SAED) pattern taken from both the ZnS:Mn film and PMN–PT substrate along the [010] direction of the ZnS:Mn film is shown in Figure 2d. The lattice constant *c* of ZnS:Mn measured from SAED is about 6.37 Å, which is close to the result from XRD. The broaden electron diffraction spots with satellites from ZnS:Mn film indicate the film has a highly preferred orientation and ZnS:Mn has a wurtzite (hexagonal) structure.

We applied a positive poling voltage of +500 V across the ZnS:Mn/PMN–PT structure to make the PMN–PT substrate positively polarized. **Figure 3**a shows the normalized light emission spectra of ZnS:Mn film by electric-field operating at 500 Hz and 200 V_{pp}. The device functions in stable and reproductive way, meaning that no obvious degradation or ZnS:Mn phosphors breakdown were found in the device during the initial process. For comparison, photoluminescence (PL) from the ZnS:Mn film is also presented in Figure 3a. The dominant peak is found at approximately 588 nm in the electric-field induced emission spectrum of ZnS:Mn, which is similar to the PL spectrum of ZnS:Mn. This indicates that the electric-field induced luminescence also results from the $^4T_1 \rightarrow {}^6A_1$ transition of Mn^{2+}. We have investigated the mechanism of the

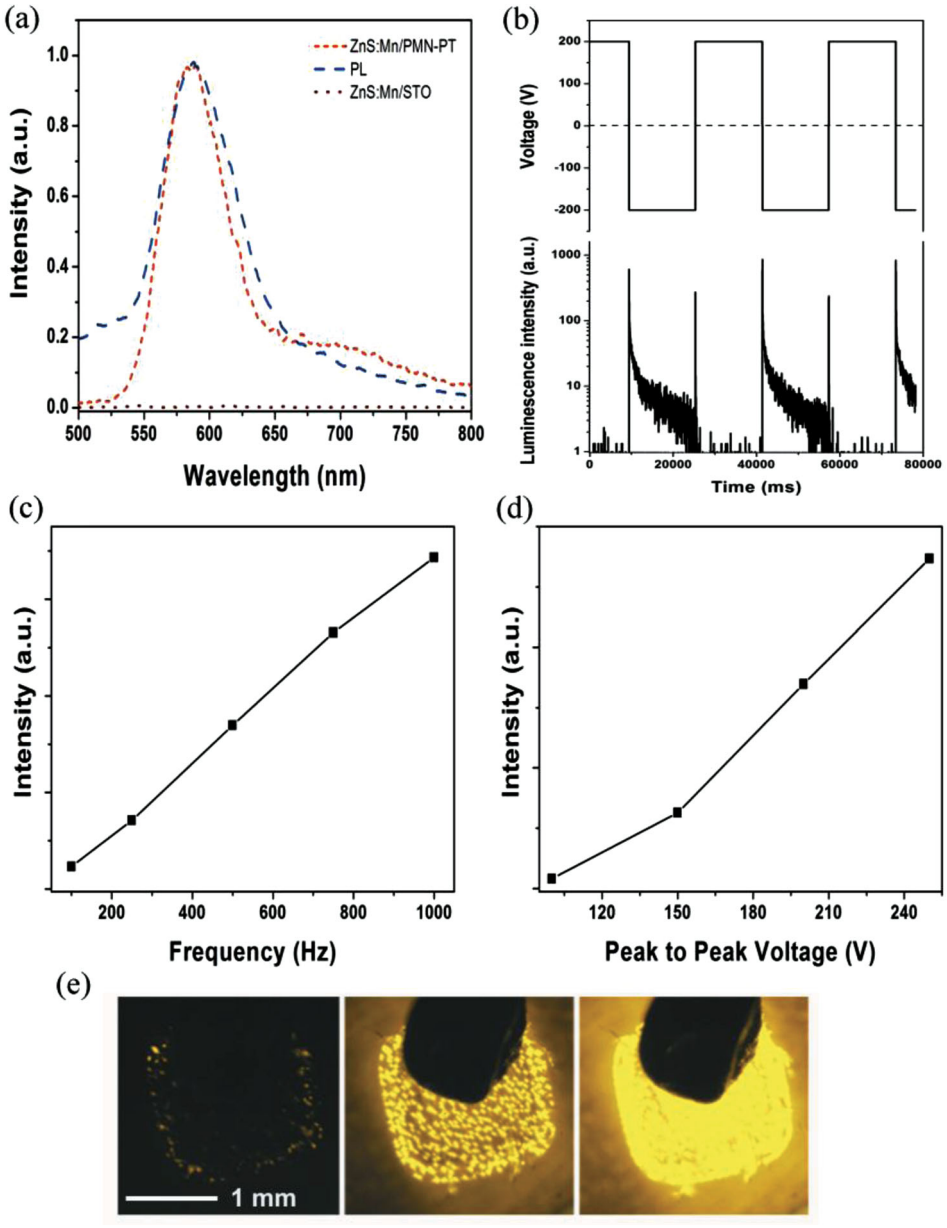

Figure 3. a) The luminescence spectra for structures with PMN–PT and STO insulating substrate operating at 200 V_{pp} and 500 Hz are presented as red dashes and brown dots, respectively. A photoluminescence of the sample excited by 320 nm is also demonstrated by the long blue dashes. b) Square electric voltage applied to the ZnS:Mn/PMN–PT structure (top), and the luminescence at a wavelength 586 nm as a function of time while the square electric-voltage is applied (bottom). c) The luminescence response as a function of frequency at 200 V_{pp}. d) The luminescence response as a function of voltage at 500 Hz. e) Light emission photographs of ZnS:Mn film (1 mm × 1 mm pixel) fabricated on PMN–PT substrate operating with peak-to-peak voltages of 50, 100, and 200 V (left to right, respectively), under the same applied frequency of 500 Hz.

luminescence in ZnS:Mn film on PMN–PT substrate. We take advantage of large converse piezoelectric effect in PMN–PT and realize in situ lattice strain on the grown ZnS:Mn film. The PMN–PT substrate was positively polarized prior to the measurements of the luminescent properties of the ZnS:Mn film. When an ac electric field less than the coercive field is applied to the polarized PMN–PT substrate, the lattice of the PMN–PT substrate will expand or contract along the direction of the electric field. Our previous studies have shown that the lattice of the PMN–PT substrate can expand and contract along the *c* axis at the same frequency as that of applied electric field.[26,29] The electric field-induced lattice displacements originate from the converse piezoelectric effect of the PMN–PT substrate. Such a modulation in the lattice parameter *c* will cause changes in the in-plane lattice parameters *a* and *b* as a result of the Poisson effect,[30] which can subsequently impose in-plane strains in the ZnS:Mn film. XRD and TEM results indicate that the ZnS:Mn film is of good quality and firmly adheres to the underlying substrate. ZnS:Mn of wurtzite structure possesses a non-central symmetric structure. Hence, the substrate-imposed strain can give rise to a piezoelectric potential. Previous research[11–21] has shown that the inner potential in semiconducting materials can modify the band structure for a p–n junction, and consequently influence the light emission performance. However, the structure of the p–n junction is not applicable to ZnS:Mn/PMN–PT samples, as the PMN–PT single crystal is an insulator with high resistance and permittivity. The inner-crystal potential can trigger the creation of an electron–hole pair, exciting an electron to escape from the valence band and reach the conduction band. Two excitation mechanisms for the Mn^{2+} are possible based on our observations. In some literature,[31] Mn^{2+} ions were observed to be more likely hole attractive. Hence, the Mn^{2+} may first trap a hole and subsequently recombine with the electron in the conduction band, resulting in Mn^{2+} in an excited state. While the Mn^{2+} returns from the excited state to ground state, an orange light is emitted[32]

$$Mn^{2+} + h^{+}\,(VB) \rightarrow Mn^{3+}$$

$$Mn^{3+} + e^{-} \rightarrow (Mn^{2+})^{*}$$

$$(Mn^{2+})^{*} \rightarrow Mn^{2+} + h\nu$$

Alternatively, the electrons of the conduction band can directly couple with the hole to form an exciton. The exciton is then bound to Mn^{2+}. Subsequent recombination of the exciton promotes the Mn^{2+} to the excited state and is followed by the light emission. It is evidentht that the strain-induced piezoelectric potential plays a crucial role in the observed luminescence of ZnS:Mn. Luminescence based on the piezo-phototronic effect and conventional ACTFEL suffer some similar physical processes, such as the impact excitation of the luminescent center and the de-excitation of the excited luminescent dopant ions. The essential difference between the two types of luminescence is the trigger fuse for these two physical phenomena. Conventional ACTFEL is generated from electrons across the interface between the phosphor and insulator layer. The electrons are accelerated by an external electric-field and excite the luminescent center or host lattice. However, in our experiment, the piezoelectric potential originates from the substrate-imposed strain on the piezoelectric host, which de-traps the electron in the valence band, and goes with the following processes. To confirm the hypothesis, a non-piezoelectric insulator strontium titanate (STO) was substituted for PMN–PT as the substrate sandwiched between ZnS:Mn and the bottom Au electrode. It was found that no obvious luminescence was observed from this sample (Figure 3a), as expected. This indicates that our observed luminescence indeed originates from the piezoelectric potential stimuli, differing from conventional ACTFEL. Some researchers have reported that ceramics or nanoparticles can emit luminescence under mechanical stress, friction, and strike.[33,34] This macroscopic mechanical stimulus-induced luminescence is termed mechanoluminescence. Apparently, it is relatively difficult to control the generation of strain from mechanical stress, friction, and strike. However, the utilization of piezoelectric PMN–PT substrate in this work provides an effective and precise approach to control over a range of strain state of the thin-films and therefore can realize strain-mediated luminescence. Furthermore, the electric-field-controllable luminescence from the ZnS:Mn/PMN–PT thin-film configuration has the potential for the development of integrated devices. It is known that the external quantum efficiency of the luminescent device is determined by not only internal quantum efficiency, but also light output coupling efficiency related to total internal reflection and the waveguiding effect of high-index material. Thus, it is much needed to optimize the design and fabrication of the device, and therefore improve the device's quantum efficiency, in the future.

Figure 3b shows the transient luminescence of the thin-film sample stimulated under a square electric voltage. The observation confirms that the strain-induced luminescence is essentially a dynamic process when a time-varying voltage is applied. Pulsed emissions were observed in response to the transient voltages. It is suggested that the emission intensity of luminescence depends on the rate of strain change induced by the applied voltage and that the largest luminescence intensity appears when the bias is switching. Similar observations have commonly been observed in the studied mechanoluminescence of ZnS:Mn.[34] Applying positive and negative bias to the sample, the lattice of PMN–PT substrate will change in an opposite manner, i.e., expanding and contracting along the *c* axis,[26] subsequently imposing a different affect on the grown ZnS:Mn film. The piezoelectric potential created by strain in the ZnS:Mn has a polarity, which may result in the different response of luminescence at the rising and falling edges in Figure 3b. Figures 3c and d show the luminescent intensity as a function of applied voltage and frequency. So, we can realize the tuning of emission intensity of ZnS:Mn thin-film in situ and in real-time by applying an ac electric field across the PMN–PT substrate, similar to our recent report regarding electric field-modulated PL.[35] The photographs in Figure 3e illustrate the obvious luminescence from a ZnS:Mn film (1 mm × 1 mm pixel) grown on PMN–PT substrate applied with different applied voltages at 500 Hz. An orange light emission can be observed by the naked eye.

Regardless of the vibration systems, resonance always results in a greater amplitude. Resonance is expected to be able to produce intense luminescence under relatively low voltages. So, further analysis was performed to characterize the

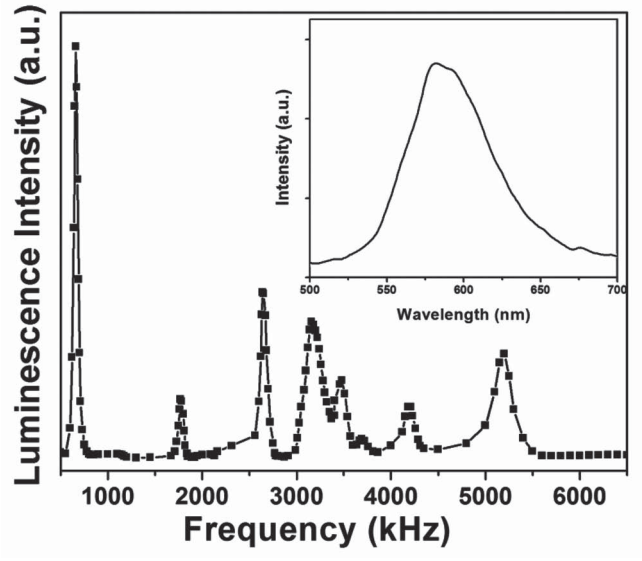

Figure 4. Frequency dependence of the luminescence intensity for ZnS:Mn film under the applied voltage 10 V_{pp}. Inset shows the luminescence spectra of ZnS:Mn operating at 650 kHz and 10 V_{pp}.

luminescence of ZnS:Mn on PMN–PT under high-frequency vibration stimuli. **Figure 4** shows the luminescence as a function of frequency when sinusoidal voltage is applied on PMN–PT. The samples were adhered on a glass plate to facilitate operation during the luminescence measurement. The intensity of luminescence shows strong dependence on the voltage frequency. The inset is the emission spectra of the ZnS:Mn film taken under an applied voltage of 10 V_{pp} at 650 kHz. The spectral profile in terms of curve shape and peak position is almost same as the observed luminescence under low-frequency stimuli. Strong frequency dependent luminescence from ZnS:Mn/PMN–PT system indicates that the resonance occurs at its nature frequency. When the PMN–PT substrate is excited by an applied voltage at its natural resonance frequencies, larger vibration amplitude occurs. Along with the fundamental plate mode resonance (around 650 kHz) and the thickness mode resonance (around 5.20 MHz), as well as their harmonics, there also appeared some minor resonances originated from the sample configuration (Figure 4). All these resonances of PMN–PT could lead to emission peaks from ZnS:Mn. Based on the observation of the frequency-dependent luminescence, we suggest that PMN–PT working at a resonant frequency can greatly promote emissions. The frequency-dependent results further rule out the probability of conventional ACTFEL. In contrast to conventional ACTFEL devices, the obtained luminescent device in this work can operate at high frequency: up to MHz.

The above results provide an indication that it is possible to realize on-chip multi-mode source integrated thin-film phosphors with piezoelectric materials after the observation of light emission from ZnS:Mn film by an external applied voltage via the converse piezoelectric effect. Many imaging technologies – including optical imaging and ultrasonic imaging – are capable of providing various information on anatomical structure or

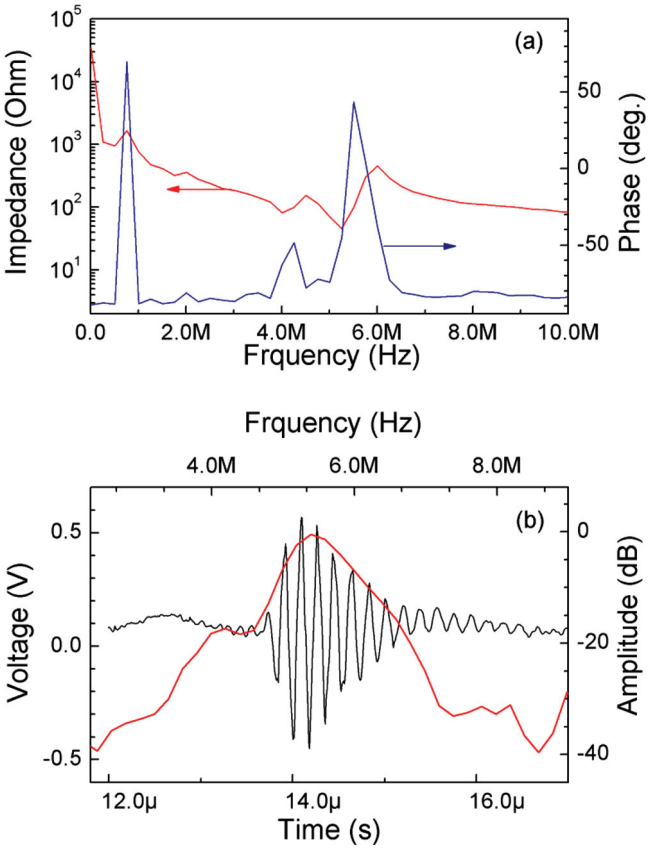

Figure 5. a) The thickness mode impedance and phase spectra for the PMN–PT single-crystal. b) Pulse-echo waveform and frequency spectrum for PMN–PT coated with ZnS:Mn film.

composition. But each imaging modality has its own merits and application limitations. Great efforts have been focused on the development of multi-modal imaging system.[22,36] There have been reports on dual-modal diagnostic devices combining optical and ultrasonic imaging, i.e., a hybrid system combines an optical fiber and an ultrasonic transducer. It would be attractive if a single source combined with light and ultrasound generation could be produced and hence integrated with detecting system. To validate the feasibility of the novel signal source, the ZnS:Mn/PMN–PT structure was poled along the thickness direction and the test signal was also applied along same direction. **Figure 5**a shows the impedance and phase spectra of the sample with PMN–PT thickness of 0.5 mm as a function of frequency in a frequency range from 0.5 to 30 MHz. It can be seen that the plate mode resonance is found at approximately 750 kHz. The thickness mode resonance frequency (f_r) and the anti-resonance frequency (f_a) can be observed at 5.25 and 6.05 MHz, respectively. The thickness electromechanical coupling coefficient k_t can be derived from[28]

$$k_t^2 = \frac{\pi}{2}\frac{f_r}{f_a}\tan\left(\frac{\pi}{2}\frac{f_a - f_r}{f_a}\right) \quad (1)$$

k_t is found to be 0.53. Figure 5b shows a pulse-echo waveform and frequency spectrum of the PMN–PT coated with ZnS:Mn film. The center frequency of the structure was found to be

about 5.48 MHz, which falls into the range of ultrasonic frequency for medical diagnostic. The fractional bandwidth at –6 dB was measured to be around 16.6%. There is plenty room to improve the performance by optimizing the fabrication technology. At any rate, the results are indicative of the dual functions, i.e., light source and ultrasound transducer in the device structure of ZnS:Mn thin film grown on PMN–PT.

In conclusion, we have demonstrated electric field-controllable luminescence of ZnS:Mn grown on piezoelectric PMN–PT substrate, based on a different working principle than conventional EL. The light emission of the ZnS:Mn is caused by the piezoelectric potential, resulting from the converse piezoelectric effect of PMN–PT substrate. Such a novel light source coupling of piezoelectric and photonic characteristics can be driven by high-frequency voltage triggering up to the MHz scale. Moreover, simultaneous generation of light and ultrasound wave is observed using a single ZnS:Mn/PMN–PT system, which offers great potential in developing a dual-modal source combing light and ultrasonic wave for a variety of applications.

Experimental Section

ZnS: Mn thin films were grown on (001) cut PMN–PT single-crystal substrate by pulsed laser deposition with a KrF excimer laser (wavelength 248 nm). The PMN–PT single-crystal was cut into plates of dimensions of 5 mm × 3 mm × 0.5 mm. The pulse repetition frequency and energy density were 5 Hz and 2 J cm^{-2}, respectively. The substrate temperature and base pressure of the vacuum chamber were fixed at 500 °C and 5 × 10^{-3} Pa. After deposition, the ZnS:Mn films were slowly cooled down to room temperature. An ITO transparent conductive electrode was grown on the top of the film at 200 °C under a 2.0 Pa oxygen pressure. A 200 nm thick Au electrode on the back of PMN–PT substrate was coated by a sputtering system at room temperature.

The XRD measurements were carried out using a four-circle Bruker D8 Discover x-ray diffractometer equipped with a four-bounce Ge (220) monochromator. TEM and SAED were performed on a JEOL 2010 electron microscope furnished with energy dispersive x-ray, operating at a voltage of 200 kV.

The polarization of the PMN–PT substrate was done using a Keithley 2410 Source-Meter with a high-voltage output. The samples were positively polarized in the thickness direction (i.e., the electric dipole moments in the PMN–PT substrate point toward the ZnS:Mn film). The AC signals applied on the sample were produced using a Keithley 3390 Arbitrary Waveform/Function generator connected with a voltage amplifier. The dielectric properties were carried out on a precision impedance analyzer 4294A (Agilent, USA). A conventional pulsed-echo response arrangement was adopted to measure the performance of the ZnS:Mn/PMN–PT structure as a transducer. The sample was connected to a Panametrics 5900PR pulser/receiver (Waltham, MA), and mounted in front of a thick stainless target with a proper distance in a water tank. An oscilloscope (HP Infinium, Agilent) was used to record the pulsed-echo signal. The luminescence measurements were recorded using an Edinburgh FLSP920 spectrophotometer. The photographs were obtained by an inverted microscope (IX-71, Olympus). For luminescence and imaging experiments, the samples were adhered on a glass plate for facilitating the operation. All measurements were carried out at room temperature.

Acknowledgements

The work was supported by the Hong Kong Polytechnic University Postgraduate Scholarship (RPR6) and Niche Areas Grant (J-BB9R). We also thank Dr. D. Zhou for the assistance in pulse-echo response measurement.

Received: December 1, 2011
Revised: January 19, 2012
Published online: March 6, 2012

[1] R. J. Walters, G. I. Bourianoff, H. A. Atwater, *Nat. Mater.* **2005**, *4*, 143.
[2] H. Takashima, K. Shimada, N. Miura, T. Katsumata, Y. Inaguma, K. Ueda, M. Itoh, *Adv. Mater.* **2009**, *21*, 3699.
[3] P. Wellenius, A. Suresh, J. F. Muth, *Appl. Phys. Lett.* **2008**, *92*, 021111.
[4] J. H. Hao, Z. D. Lou, I. Renaud, M. Cocivera, *Thin Solid Films* **2004**, *467*, 182.
[5] M. Shao, L. Yan, H. P. Pan, I. Ivanov, B. Hu, *Adv. Mater.* **2011**, *23*, 2216.
[6] K. Chung, C.-H. Lee, G.-C. Yi, *Science* **2010**, *330*, 655.
[7] S. Pimputkar, J. S. Speck, S. P. Denbaars, S. Nakamura, *Nat. Photon.* **2009**, *3*, 180.
[8] M. Vasilopoulou, D. Georgiadou, G. Pistolis, P. Argitis, *Adv. Funct. Mater.* **2007**, *17*, 3477.
[9] Y. J. Hong, C. H. Lee, A. Yoon, M. Kim, H. Y. Seong, H. J. Chung, C. Sone, Y. J. Park, G. C. Yi, *Adv. Mater.* **2011**, *23*, 3284.
[10] N. Holonyak, S. F. Bevacqua, *Appl. Phys. Lett.* **1962**, *1*, 82.
[11] Z. L. Wang, *Nano Today* **2010**, *5*, 540.
[12] Z. L. Wang, J. H. Song, *Science* **2006**, *312*, 242.
[13] Z. L. Wang, *Adv. Mater.* **2007**, *19*, 889.
[14] Y. F. Hu, Y. Zhang, C. Xu, G. Zhu, Z. L. Wang, *Nano Lett.* **2010**, *10*, 5025.
[15] S. Xu, Y. Qin, C. Xu, Y. G. Wei, R. Yang, Z. L. Wang, *Nat. Nanotechnol.* **2010**, *5*, 366.
[16] S. N. Cha, J.-S. Seo, S. M. Kim, H. J. Kim, Y. J. Park, S.-W. Kim, S.-W Kim, J. M. Kim, *Adv. Mater.* **2010**, *22*, 4726.
[17] P. Fei, P.-H. Yeh, J. Zhou, S. Xu, Y. F. Gao, J. H. Song, Y. D. Gu, Y. Y. Huang, Z. L. Wang, *Nano Lett.* **2009**, *9*, 3435.
[18] S.-S. Kwon, W.-K. Hong, G. Jo, J. Maeng, T.-W. Kim, S. Song, T. Lee, *Adv. Mater.* **2008**, *20*, 4557.
[19] Q. Yang, X. Guo, W. H. Wang, Y. Zhang, S. Xu, D. H. Lien, Z. L. Wang, *ACS Nano* **2010**, *4*, 6285.
[20] J. Zhou, P. Fei, Y. D. Gu, W. J. Mai, Y. F. Gao, R. S. Yang, G. Bao, Z. L. Wang, *Nano Lett.* **2008**, *8*, 3973.
[21] Q. Yang, W. H. Wang, S. Xu, Z. L. Wang, *Nano Lett.* **2011**, *11*, 4012.
[22] Y. Sun, J. Park, D. N. Stephens, J. A. Jo, L. Sun, J. M. Cannata, R. M. G. Saroufeem, K. K. Shung, L. Marcu, *Rev. Sci. Instrum.* **2009**, *80*, 065104.
[23] C. B. Thomas, W. M. Cranton, *Appl. Phys. Lett.* **1993**, *63*, 3119.
[24] W. Wood, J. E. Halpert, M. J. Panzer, M. G. Bawendi, V. Bulovic, *Nano Lett.* **2009**, *9*, 2367.
[25] R. Zhang, B. Jiang, W. W. Cao, *Appl. Phys. Lett.* **2003**, *82*, 787.
[26] R. K. Zheng, Y. Wang, J. Wang, K. S. Wong, H. L. W. Chan, C. L. Choy, H. S. Luo, *Phys. Rev. B.* **2006**, *74*, 094427.
[27] E. J. Guo, J. Gao, H. B. Lu, *Appl. Phys. Lett.* **2011**, *98*, 081903.
[28] D. Zhou, K. F. Cheung, Y. Chen, S. T. Lau, Q. F. Zhou, K. K. Shung, H. S. Luo, J. Y. Dai, H. L. W. Chan, *IEEE Trans. Ultrason. Ferroelectr. Freq. Control* **2011**, *58*, 477.
[29] R. K. Zheng, Y. Wang, H. L. W. Chan, C. L. Choy, H. S. Luo, *Appl. Phys. Lett.* **2007**, *90*, 152904.

[30] S. P. Timoshenko, J. N. Goodier, *Theory of Elasticity*, McGraw-Hill, New York **1987**.
[31] T. Hoshiba, H. Kawai, *Jpn. J. Appl. Phys.* **1980**, *19*, 267.
[32] J. F. Suyver, S. F. Wuister, J. J. Kelly, A. Meijerink, *Nano Lett.* **2001**, *1*, 429.
[33] X. Wang, C.-N. Xu, H. Yamada, K. Nishikubo, X.-G. Zheng, *Adv. Mater.* **2005**, *17*, 1254.
[34] B. P. Chandra, C. N. Xu, H. Yamada, X. G. Zheng, *J. Lumin.* **2010**, *130*, 442.
[35] J. H. Hao, Y. Zhang, X. H. Wei, *Angew. Chem., Int. Ed.* **2011**, *50*, 6876.
[36] G. Zhang, Y. L. Liu, Q. H. Yuan, C. H. Zong, J. H. Liu, L. H. Lu, *Nanoscale* **2011**, *3*, 4365.